Resonance phenomena in an annular array of underdamped Josephson junctions

I. R. Rahmonov [1,2] J. Tekić [3,*] P. Mali,[4] A. Irie,[5] A. Plecenik,[6] and Yu. M. Shukrinov[1,7]

[1]*Bogoliubov Laboratory of Theoretical Physics, Joint Institute for Nuclear Research, Dubna, Moscow Region 141980, Russia*

[2]*Umarov Physical Technical Institute, TAS, Dushanbe 734063, Tajikistan*

[3]*Department of Theoretical and Condensed Matter Physics – 020, "Vinča" Institute of Nuclear Sciences – National Institute of the Republic of Serbia, University of Belgrade, P.O. Box 522, 11001 Belgrade, Serbia*

[4]*Department of Physics, Faculty of Science, University of Novi Sad, Trg Dositeja Obradovića 4, 21000 Novi Sad, Serbia*

[5]*Department of Electrical and Electronic Systems Engineering, Utsunomiya University, 7-1-2 Yoto, Utsunomiya 321-8585, Japan*

[6]*Department of Experimental Physics, Comenius University in Bratislava, 814 99 Bratislava, Slovakia*

[7]*Dubna State University, Dubna 141980, Russia*

(Received 4 November 2019; revised manuscript received 14 April 2020; accepted 14 May 2020; published 28 May 2020)

The appearance and origin of resonance phenomena are studied in an annular system of underdamped Josephson junctions. If no fluxon is trapped in the system, the dynamics is governed by the motion of fluxon-antifluxon pairs. If, on the other hand, trapped fluxons are present, in addition to their motion, the system can also exhibit the simultaneous motion of trapped fluxons and fluxon-antifluxon pairs. Locking between the rotating excitations (fluxons and antifluxons) and the Josephson frequency leads to the appearance of zero-field steps in the current-voltage characteristics, whose number is determined by the number of junctions and the total number of excitations present in the system. The obtained results clearly show that the branching of zero-field steps due to resonance between the rotating excitations and plasma oscillations in their tails appears only at the lower steps and completely disappears at the higher steps. A comparative analysis between systems without and those with trapped fluxons shows a correlation between their current-voltage characteristics. From a high-resolution analysis some special features of zero-field steps emerge such as an additional branch due to resonance between the pulsating fluxon and the Josephson frequency. Examination of systems with the same number but different types of excitations further reveals that their dynamics is determined not only by the number, but also by the type of excitations, i.e., systems with the same number but different types of excitations have different current-voltage characteristics.

DOI: 10.1103/PhysRevB.101.174515

I. INTRODUCTION

Resonance phenomena in Josephson junction (JJ) systems have been an active research topic in science and technology for years. From the fundamental point of view JJs are excellent devices for studies of nonlinear dynamics of discrete systems, as they represent an experimental realization of the Frenkel-Kontorova model (discrete sine-Gordon model) [1–7]. At the same time, regarding their applications, JJs are promising devices for the development of various fields, from the generation and detection of electromagnetic radiations in the very low terahertz range [1], quantum information technologies [8–18], and superconducting metamaterials [19] to fields as distant as biology [20].

Systems described by sine-Gordon equations can exhibit three types of dynamical solutions: small amplitude waves, solitons, and breathers [1,2]. In JJ systems, the soliton solution has a real physical meaning since it corresponds to a quantum of flux trapped in a junction also called a fluxon or Josephson vortex [5,6,21]. The idea that a fluxon behaves as a particlelike solitary wave, which can be manipulated and controlled, motivated the creation of a new logic circuit by using Josephson fluxons as elementary bits of information [11–18]. In the creation of new logic elements, particularly important are the long Josephson junctions described by the continuous sine-Gordon equation and the Josephson junction parallel array described by its discrete counterpart, i.e., the Frenkel-Kontorova model [2–4]. A very good overview of the most prominent fluxon dynamics results in both natural and man-made systems can be found in Ref. [1].

The dynamics of long Josephson junctions have been the subject of numerous theoretical and experimental studies [1,22,23]. However, in long JJs, the motion of fluxons depends on the geometry and boundaries of the junctions, which act as a mirror reflecting the fluxon into the antifluxon (this process can be viewed as a fluxon-antifluxon collision). Thus, the current-voltage (I-V) characteristics of long JJs can be very complicated, which makes studies of fluxon dynamics very challenging. These problems led to the creation of annular Josephson junctions as well as annular systems of Josephson junctions with a ring-shaped geometry [24]. Annular junctions provide an undisturbed and very tunable fluxon motion, which today makes them an ideal system for studies of fluxon dynamics [25–34].

*jasminat@vin.bg.ac.rs

One of the well-known properties of JJ systems is the appearance of resonant steps in the current-voltage characteristics in the absence of any external radiation [5,35,36]. Though the first experimental indication of their existence was reported earlier [37], the name zero-field steps (ZFSs) for the observed resonant structures and the first theoretical explanation in terms of vortex motion inside the long junction were introduced by Fulton and Dynes in their pioneering work on the long Josephson junction [5]. The ever present need for undisturbed fluxon motion without collisions further motivated studies of resonance phenomena in annular systems [24–26,29,32], where the appearance of ZFSs can be interpreted in terms of the circulating motion of fluxons and antifluxons.

In this paper, we examine the underdamped dynamics of an annular array of Josephson junctions (AAJJs), focusing particularly on the origin and the appearance of various resonance phenomena in the absence of external radiation. Zero-field steps have been studied previously in annular systems of Josephson junctions [25,27], however, these studies have focused only on systems with one trapped fluxon, and the small region of *I*-*V* characteristics, i.e., the one corresponding to the first (lowest) ZFS, has usually been examined. In contrast to these studies [25,27], here we examine the resonance phenomena in the AAJJ in various cases: without trapped fluxons, where the dynamics is characterized by the motion of FAPs, and with trapped fluxons. Our analysis is performed in a wide range of currents and voltages—from the regions which exhibit ZFSs all the way to the high-voltage regions where ZFSs disappear—in order to get a full picture of their behavior. This is particularly important in the case of trapped fluxons. Namely, if we perform the analysis in the same way as done previously [25,27], we would consider only the dynamics, which are governed by the motion of trapped fluxons. However, going beyond that limit and into higher voltages, in addition to trapped fluxons, FAPs start to appear and the dynamics is now characterized by the simultaneous motion of trapped fluxons and fluxon-antifluxon pairs, which completely changes the system behavior. In order to understand some of the properties of ZFSs we also perform a comparative analysis between systems with different numbers and systems with different types of moving excitations. This enables us to observe some new properties of AAJJs which otherwise could not be seen, such as the correlation between the *I*-*V* characteristics of a system without and those of a system with trapped fluxons. Our results also show that the dynamics of the AAJJ depends not only on the number but also on the type of excitations, i.e., systems with the same total number of excitations but different types will have different *I*-*V* characteristics.

The paper is organized as follows. The model is introduced in Sec. II, while the simulation results are presented in Secs. III–VII. The influence of the discreteness of the system on the appearance of ZFSs is examined in Sec. III, while their branching is analyzed in Sec. IV. The correlation between the current-voltage characteristics in the case without and those in the case with trapped fluxons is presented in Sec. V. The appearance of a fine structure or an additional branch in the current-voltage characteristics due to the presence of a pulsating fluxon is shown in Sec. VI. A comparative analysis of systems with the same number but different types of excitations is performed in Sec. VII. Finally, Sec. VIII concludes the paper.

II. MODEL

We consider an annular parallel array of N underdamped Josephson junctions [25]. The total length of a chain is $L = Na$, where a is the distance between neighboring junctions. In order to derive dynamical equations for the description of such discrete systems, we start from the equations for a continuous annular JJ. In fact, the annular JJ is actually a long JJ with periodic boundary conditions, and so, we start from the equations for a long JJ. A Josephson junction is considered to be long or short if its length is longer or shorter than the Josephson penetration depth $\lambda_J = \sqrt{\hbar S/(2e\mu_0 D I_c)}$, respectively. Here S is the surface area of the superconducting layer, e is the electron charge, μ_0 is the magnetic constant, $D = 2\lambda_L + d$ is the effective magnetic thickness, λ_L is the London penetration depth, and d is the thickness of insulating layers.

According to the resistively and capacitively shunted junction model (RCSJ) [38,39] the total current through the junction is the sum of the Josephson supercurrent, quasiparticle (resistive normal) current, and displacement (capacitive) current,

$$I = I_s + I_{\rm qp} + I_d,$$
$$I_s = I_c \sin\varphi, \quad I_{\rm qp} = \frac{V}{R}, \quad I_d = C\frac{dV}{dt}, \tag{1}$$

where φ and V are the phase difference and voltage across the junction, while R and C are the resistance and capacitance of the JJ, respectively. The voltage V is given by the Josephson relation

$$V = \frac{\hbar}{2e}\frac{d\varphi}{dt} = \frac{\hbar}{2e}\omega_J, \tag{2}$$

where ω_J is the Josephson frequency. In the case of the long JJ, the surface current I_{sf} along the superconducting layer, given as

$$I_{\rm sf} = I_c\lambda_J^2\frac{\partial^2\varphi}{\partial x^2}, \tag{3}$$

should also be taken into account.

Using Eqs. (1), (2), and (3), the total or bias current I through the junction can be written as

$$\frac{\hbar C}{2e}\frac{\partial^2\varphi}{\partial t^2} - I_c\lambda_J^2\frac{\partial^2\varphi}{\partial x^2} + I_c\sin\varphi + \frac{\hbar}{2eR}\frac{\partial\varphi}{dt} = I. \tag{4}$$

In the normalized form, Eq. (4) for the phase difference in JJs can be simplified as

$$\frac{\partial^2\varphi}{\partial t^2} - \frac{\partial^2\varphi}{\partial x^2} + \sin\varphi + \alpha\frac{\partial\varphi}{\partial t} = I, \tag{5}$$

where the time is normalized with respect to the inverse plasma frequency ω_p^{-1}, $\omega_p = \sqrt{2\pi I_c/(\Phi_0 C)}$, the coordinate is normalized with respect to λ_J, and the bias current I with respect to the critical current I_c. The dissipation parameter is given as $\alpha = \sqrt{\Phi_0/(2\pi I_c R^2 C)}$, where L_0, C, and R are the inductance, capacitance, and differential resistance of a single cell, respectively, and $\Phi_0 = \frac{h}{2e}$ is the flux quantum

[40]. Equation (5) represents the well-known perturbed sine-Gordon equation. The boundary conditions for the long JJ described by Eq. (5) have the form $\partial\varphi/\partial x|_{x=0} = \partial\varphi/\partial x|_{x=L} = B_{\rm ext}$, which for the annular case are periodic, i.e., $\varphi(x=0) = \varphi(x=L) + 2\pi M$, where $B_{\rm ext}$ is the external magnetic field and M represents the number of trapped fluxons inside the system.

The annular system that we consider here can be described by the discrete version of the perturbed sine-Gordon equation, which is well known as the dissipative Frenkel-Kontorova model [2],

$$\frac{d^2\varphi_i}{dt^2} - \frac{\varphi_{i+1} - 2\varphi_i + \varphi_{i-1}}{a^2} + \sin\varphi_i + \alpha\frac{d\varphi_i}{dt} = I, \quad (6)$$

where φ_i is the phase difference across the ith junction. The coupling between the neighboring junctions is described by the constant $\frac{1}{a^2}$, where $a = \sqrt{2\pi L_0 I_c/\Phi_0}$ is the discreteness parameter, i.e., the distance between two junctions normalized to the λ_J.

Equation (6) can be linearized around a solution consisting of a traveling kink (fluxon) and a small linear wave (perturbation) [25]. The dispersion law for linearized waves is given as

$$\omega_m = \sqrt{1 + \frac{4}{a^2}\sin^2\left(\frac{\pi m a}{L}\right)}, \quad (7)$$

where m is an integer.

In order to calculate the I-V characteristics of the AAJJ we have used Eq. (6) and the Josephson relation,

$$V_i = \frac{d\varphi_i}{dt} = \omega_J, \quad (8)$$

where V_i is the voltage of the ith junction normalized to $V_0 = \hbar\omega_p/2e$, and the Josephson frequency ω_J is normalized to the plasma frequency ω_p.

Our numerical simulations were performed for periodic boundary conditions, which in the discrete case have the form

$$\varphi_{N+1} = \varphi_1 + 2\pi M, \quad \varphi_0 = \varphi_N - 2\pi M, \quad (9)$$

where the spatial points $i = 0$ and $i = N+1$ are assumed to be equivalent to $i = N$ and $i = 1$. We have applied the well-known procedure used in Refs. [41] and [42]. The algorithm for calculating the I-V characteristics consists of several stages. First, for the given value of the bias current I, Eqs. (6) and (8) are solved numerically in the time interval $[0, T_{\rm max}]$ using the fourth-order Runge-Kutta method with the corresponding boundary conditions, (9), and the initial conditions $\varphi_i(0) = 0, V_i(0) = 0$ at $I = 0$. As a result we obtained the time dependence of $\varphi_i(t)$ and $V_i(t)$ for a fixed value of the bias current. Then, using the expression

$$\langle V_i\rangle = \frac{1}{T_{\rm max} - T_{\rm min}}\int_{T_{\rm min}}^{T_{\rm max}} V_i(t)dt, \quad (10)$$

where $T_{\rm min}$ is the time necessary for the system to reach steady state, we calculated the average voltage for each junction in the system. Further, the total average voltage V was obtained using the expression $V = \sum\langle V_i\rangle/N$. In this way, for a given value of the bias current I the corresponding voltage V was found. Next, we changed the bias current for some value ΔI and repeated the above procedure in order to obtain the next point. By repeating this procedure for every value of the current, the I-V characteristic was produced. We note that the solutions $\varphi_i(T_{\rm max})$ and $V_i(T_{\rm max})$ obtained for the time $T_{\rm max}$ at certain values of I were used as the initial condition for the calculation of the next point at the bias current value $I + \Delta I$.

The magnetic field in the array has been calculated by the expressions

$$B_1 = \frac{\varphi_1 - \varphi_N + 2\pi M}{a}, \quad B_i = \frac{\varphi_i - \varphi_{i-1}}{a}, \quad (11)$$

where B_i is normalized to $B_0 = \hbar c/(2eD\lambda_J)$. During our analysis, calculation of the magnetic-field time dependence in JJs was often necessary in order to understand the origin of the observed features in the I-V characteristics.

III. ZERO-FIELD STEPS

In the AAJJ that we consider, in the absence of any external radiation, rotating excitations (fluxons and antifluxons) pass repeatedly through the junctions, which leads to resonance between the circulating excitations and the Josephson frequency. The signature of this effect is the zero-field steps (ZFSs) in the I-V characteristics of the system. Depending on the system properties and the circulating excitations, these steps can exhibit various properties.

A. Zero-field steps in systems near a continuum

In nonlinear systems, which exhibit resonance phenomena, discreteness plays an important role. Let us then examine first how discreteness of the AAJJ affects the zero-field steps. We start with a case close to the continuum limit. If we have an AAJJ of length $L = Na = 10$, then the near-continuum limit can be achieved by placing $N = 100$ junctions at the distance $a = 0.1$ along the circle. In Fig. 1 the current-voltage characteristics of an annular system with 100 Josephson junctions is presented for $M = 0$ [Fig. 1(a)] and $M = 1$ [Fig. 1(b)], while the result for the long Josephson junction is shown in Fig. 1(c) for comparison. The presented curves are produced in the following way: starting from 0, the current is increased until the system transfers to the high-voltage state. Then it is decreased to 0, revealing a staircase structure; after that it is increased again till the system is in the high-voltage state. From there, the current is decreased to the first step. From the first step it is again increased to the high-voltage state, and from there it is decreased to the next step. In this way, the current is swept up and down several times, and the procedure repeated for all the steps.

These steps in Fig. 1 represent the well-known ZFSs that appear when the voltage V, i.e., the Josephson frequency, satisfies the resonant condition $\omega_J = \frac{2\pi nu}{L}$, where u is the speed of a moving fluxon (antifluxon). Here, n is the total number of excitations in the system, which can be written as $n = n_f + n_{\rm af} = 2n_p + M$, where n_f, $n_{\rm af}$, and n_p represent the number of fluxons, antifluxons, and fluxon-antifluxon pairs, respectively.

The AAJJ is a topologically closed system, therefore the number of trapped fluxons M must be conserved and new fluxons can be created only in the form of FAPs [34]. In the case where $M = 0$ (there are no trapped fluxons), the

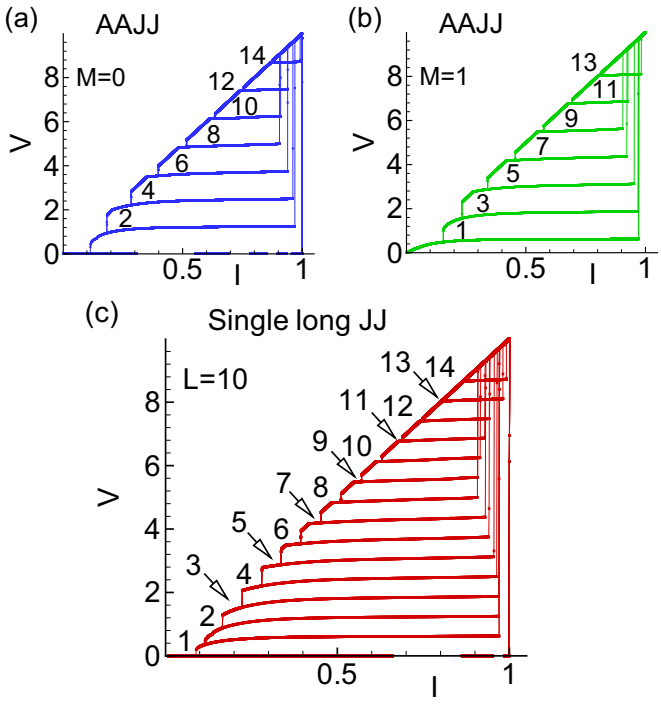

FIG. 1. Current-voltage characteristics of an annular array of Josephson junctions for $N = 100$, $a = 0.1$, $\alpha = 0.1$, and (a) $M = 0$ and (b) $M = 1$. (c) The I-V characteristics of a single long JJ. Numbers mark the total numbers of fluxons and antifluxons in the system, n.

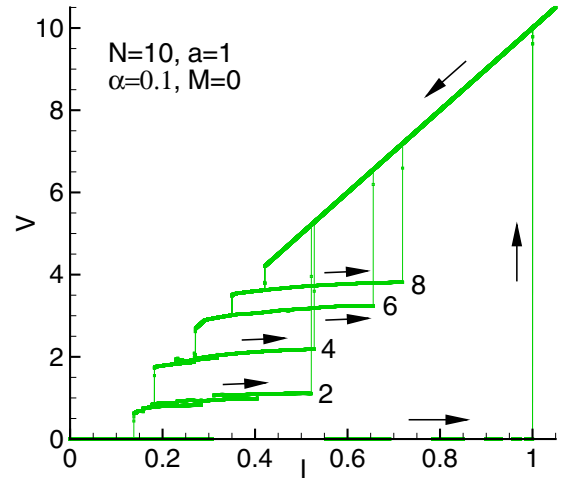

FIG. 2. Current-voltage characteristic of an annular array of Josephson junctions for $N = 10$, $a = 1$, $\alpha = 0.1$, and $M = 0$. Numbers mark the total numbers of fluxons and antifluxons. Arrows show the direction in which the current was changed.

dynamics is characterized by the motion of FAPs. Thus, in Fig. 1(a) the system exhibits only even mode resonances, where n is an even number, which corresponds to the number of fluxons and antifluxons created in pairs in the system. If we introduce one fluxon, in which case $M = 1$, we can see in Fig. 1(b) that only odd mode resonances appear, where n corresponds to the sum of the trapped fluxon and the number of fluxons and antifluxons, which come in pairs. On the other hand, the long JJ in Fig. 1(c) is not topologically closed, and it can exhibit both even and odd mode resonances.

B. Zero-field steps in discrete systems

In highly discrete systems the fluxon dynamics changes significantly. In order to discretize our system, we reduce the number of junctions to $N = 10$, while keeping the same total length $L = 10$ ($a = 1$) as in the previous case. In Fig. 2 the I-V characteristic for the case $M = 0$, where there are no fluxons trapped in the system, is presented. The curves are produced following the same procedure as for Fig. 1. In this case, the resonances come from the motion of FAPs, and the four ZFSs correspond to $n = 2, 4, 6$, and 8. If we compare this result with the one in Fig. 1(a), we can see that in the highly discrete case the number of steps is significantly reduced. This reduction of resonances comes from the fact that in order for a resonance to appear there should be a certain balance between the number of rotating excitations and the junctions in the system, i.e., the existence of stable fluxon-antifluxon pairs requires that the system is sufficiently large to permit the pair dynamics [33]. When the number of rotating fluxons and antifluxons increases, the time interval between their two consecutive passages is reduced. Consequently they are constantly passing through the junctions at a frequency much higher than ω_J, leaving no time for any resonance to appear. Further, we present some specific phenomena that we observed in our examination of ZFSs.

IV. BRANCHING OF ZERO-FIELD STEPS

If we perform a high-resolution analysis of the zero-field steps in Fig. 2, a complex structure is revealed. The enlarged regions of the I-V curves corresponding to each of four ZFSs are presented in Figs. 3(a)–3(d), respectively. The first two steps, in Figs. 3(a) and 3(b), exhibit *branching*. Namely, an excitation moving through the system excites small-amplitude linear waves in its tail, which are called Josephson plasma waves due to their plasma-type dispersion relation [see Eq. (7)]. The resonance appears due to frequency locking between the moving excitation and the small-amplitude oscillations or plasma waves (created by its motion), which results in the appearance of a series of branches at the zero-field steps in the I-V characteristics of the junction. While the ZFSs appear in both continuous and discrete systems, branching can be observed only in discrete ones [25,27]. When $M = 0$, the dynamics is characterized by the motion of FAPs, i.e., equal numbers of fluxons and antifluxons are circling in the opposite direction to each other along the AAJJ. A branch of order m appears when two consecutive passings of excitations through a junction correspond to the mth oscillation of the plasma (linear) wave. As shown in Fig. 3(a), for $n = 2$, where one pair, i.e., one fluxon and one antifluxon, rotate, the ZFS beside the main branch, which corresponds to the frequency $\omega_J = 1.107$, also has additional branches, corresponding to the frequencies $\omega_J = 0.985$, 0.882, 0.823, 0.69, and 0.635. For two FAPs in the system in Fig. 3(b), the position of the ZFS $n = 4$ corresponds to the frequency $\omega_J = 2.185$, with an additional two branches corresponding to the frequencies $\omega = 1.977$ and 1.87. On the other hand, in Figs. 3(c) and 3(d)

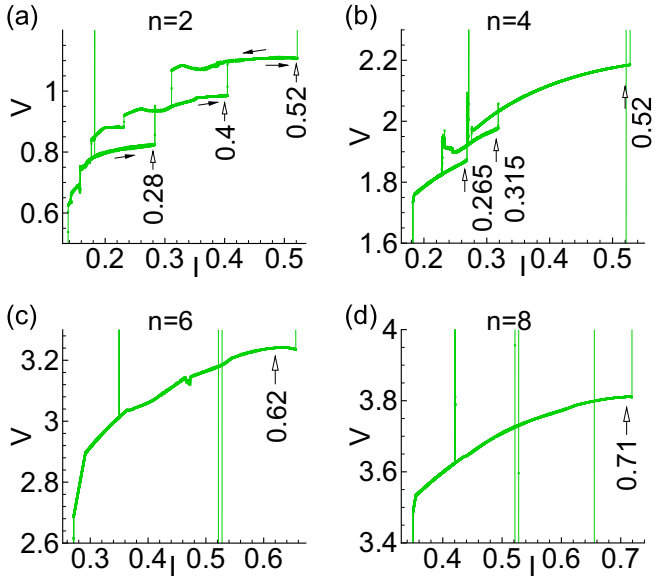

FIG. 3. High-resolution plots of the ZFSs shown in Fig. 2 for (a) $n = 2$, (b) $n = 4$, (c) $n = 6$, and (d) $n = 8$. Arrows mark the value of I at the end of each branch. Other parameters are the same as in Fig. 2.

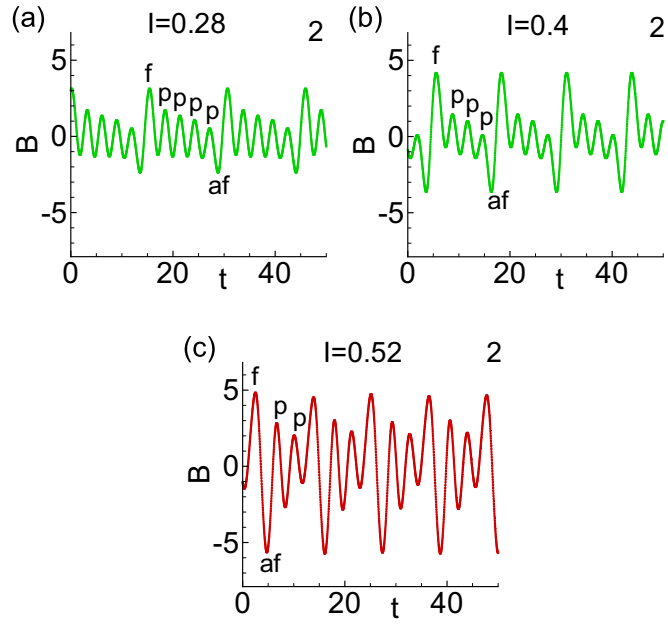

FIG. 4. Time dependence of the magnetic field B corresponding to the first three branches of the $n = 2$ ZFS with $\omega = 1.107$, 0.985, and 0.823 measured at $I = 0.28$, 0.4, and 0.52 in (a), (b), and (c), respectively. The oscillations corresponding to the fluxon, antifluxon, and plasma modes are labeled "f," "af," and "p."

no branching appears in the case of ZFSs with $n = 6$ ($\omega_J = 3.234$) and $n = 8$ ($\omega_J = 3.81$), respectively.

Let us now examine the three highest branches, $\omega_J = 1.107$, 0.985, and 0.823, in Fig. 3(a) and analyze the time dependence of the magnetic field B at the end of each branch for the values of the current I marked by arrows. The time dependence of magnetic field B at different branches of the $n = 2$ ZFS is presented in Fig. 4. For the lowest branch in Fig. 4(a), we can see that each consecutive passage of a fluxon (an antifluxon) corresponds to the fifth plasma oscillation. At the next branch, in Fig. 4(b), as the speed and the frequency of the moving fluxon increase, the time between two consecutive passages of excitations decreases, and the branch appears due to the resonance with the fourth plasma oscillation. In Fig. 4(c), which corresponds to the third branch, the speed of the fluxon and antifluxon increases further so that their motion locks with the third plasma oscillation.

Examination of the time dependence of the magnetic field can also give us an answer to why the branching is most prominent for $n = 2$ in Fig. 3(a), and as the number of pairs, i.e., fluxons and antifluxons, increases to $n = 4$ in Fig. 3(b), the number of branches decreases, completely disappearing for $n = 6$ and 8 in Figs. 3(c) and 3(d), respectively. In Fig. 5, the time dependence of magnetic field B corresponding to zero-field steps for $n = 2$, 4, 6, and 8 is presented. The magnetic field is measured at the resonant point (the end) of each step. If only one or two FAPs are moving, such as in Figs. 5(a) and 5(b), respectively, the time between each passage of a fluxon or an antifluxon is long enough so that plasma oscillations can synchronize with their motion. As the number of FAPs increases, the time between each passage decreases more and more. A large number of fluxons and antifluxons will therefore leave no time for plasma oscillations between each of their passages as we can see in Figs. 5(c) and 5(d), and consequently, there will be no resonance.

Resonances between the fluxon and the plasma waves have been studied previously in annular systems of underdamped Josephson junctions with one trapped fluxon [25], where the analysis focused only on the region of the I-V characteris-

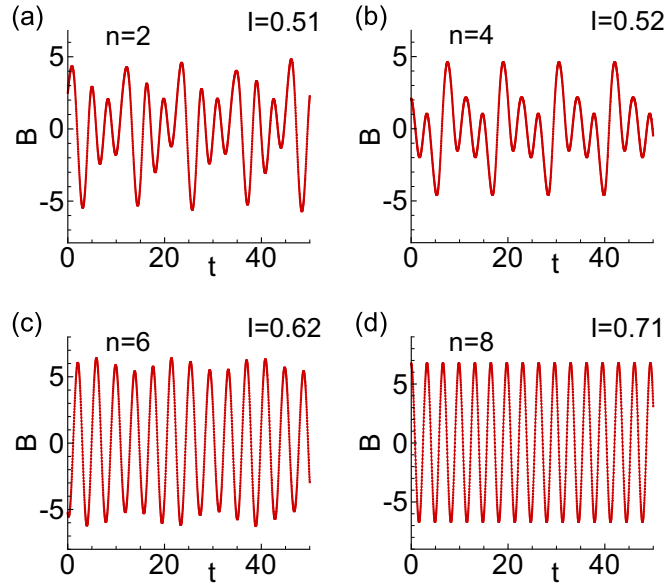

FIG. 5. Time dependence of the magnetic field B at the zero-field steps (a) $n = 2$, (b) $n = 4$, (c) $n = 6$, and (d) $n = 8$, measured at the value of current I, which corresponds to the resonant point at the end of each step.

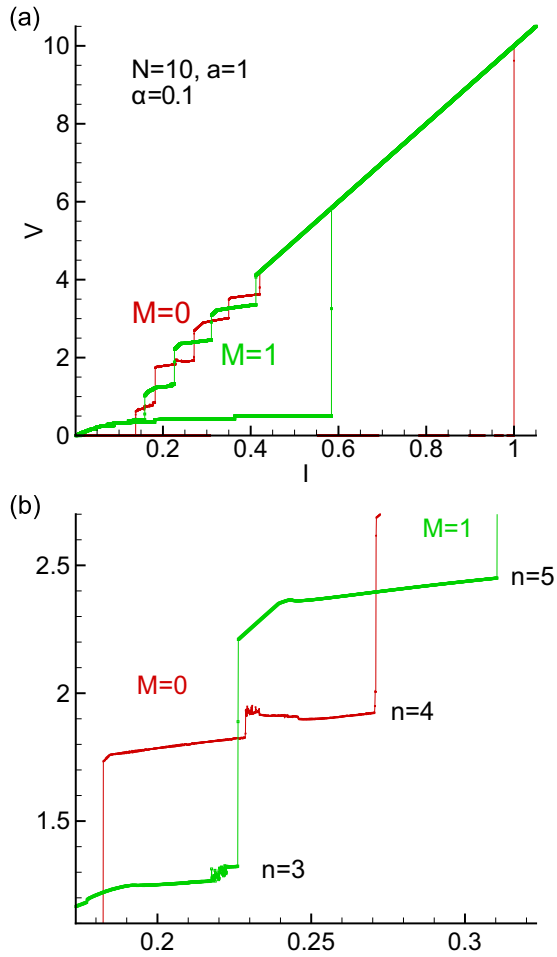

FIG. 6. (a) Current-voltage characteristics of an annular array of Josephson junctions for $N = 10$, $a = 0.1$, $\alpha = 0.1$, and $M = 0$ (red) and $M = 1$ (green). (b) High-resolution plot of the cross section between the two curves.

tics, which corresponds to the first step, i.e., one circulating fluxon, and an examination of the voltage-time dependence was performed. In our case, instead of the voltage it is more appropriate to use the magnetic-field time dependence since in this case fluxons can be distinguished from antifluxons.

V. CORRELATION BETWEEN THE STEP FOR $M = 0$ AND THE STEP FOR $M = 1$

So far, we have presented only the results obtained for $M = 0$, but we have also analyzed systems with trapped fluxons, $M \neq 0$. In Fig. 6 the current-voltage characteristics for the cases $M = 0$ and $M = 1$ are presented. As in the case for $M = 0$, for $M = 1$, in Fig. 6(a), four ZFSs will also appear, but this time only for odd values of n ($n = 1$, 3, 5, and 7), so that $n = 1$ corresponds to one rotating fluxon, $n = 3$ to one fluxon and one fluxon-antifluxon pair, etc. In the high-voltage state there is no difference between the curve for $M = 0$ and that for $M = 1$, however, in the region of ZFSs the curves intersect each other. The steps for even values of n ($M = 0$) alternate with the steps for odd values of n ($M = 1$) passing in between each other.

Interestingly, the examination of the I-V characteristics of the AAJJ with one trapped fluxon ($M = 1$) can help us understand some of the features which appear in the ZFSs when $M = 0$. Namely, the high-resolution analysis of the I-V characteristics for $M = 0$ reveals another specific property. In Fig. 6(b), we see a fine structure (a small peak), which appears at step $n = 4$, at $I = 0.23$. The origin of this effect can be understood from the comparative analysis of the I-V curves for both values of M. As we can see, the appearance of this defect at step $n = 4$ is at the current value ($I = 0.23$) for which the I-V curve for $M = 1$ changes from the $n = 5$ to the $n = 3$ state. For given system parameters the ability of the annular Josephson junction to exhibit a certain number of FAPs is determined by the current I. Thus, as the current is decreased from the high-voltage state, at some value of I, the AAJJ transfers to the state $n = 8$ (four fluxons and four antifluxons), and as we decrease I further, we can see that at certain values of the current, the AAJJ can be in states with $n = 7, 6, \ldots, 1$ excitations. In Fig. 6(b), at step $n = 4$ ($M = 0$), we have two fluxon-antifluxon pairs moving along the AAJJ, and when the current decreases to the value $I = 0.23$, the AAJJ is in the I-V region, which corresponds to the $n = 3$ state. However, it is impossible for the AAJJ to transfer to that state due to conservation of M ($n_f = n_{\rm af}$ for $M = 0$). On the contrary, the two pairs will, due to their inertia, continue moving till the current decreases to the value at which the system is reduced to the $n = 2$ state with only one FAP. Also in Fig. 6(b), we can see that the curve for $M = 1$ is slightly shifted to the right compared to the curve for $M = 0$. This might be due to the inertial effect, since for $M = 1$ the system contains one more fluxon in addition to fluxon-antifluxon pairs, and more fluxons will simply have more inertia. Thus, when the current is decreased, three fluxons and two antifluxons ($n = 5$) would keep moving longer than two fluxons and two antifluxons ($n = 4$).

VI. A PULSATING FLUXON

Let us now examine step $n = 1$ for an AAJJ with one trapped fluxon, $M = 1$. The high-resolution plot of the I-V curve in Fig. 6 corresponding to step $n = 1$ (one-fluxon state) is presented in Fig. 7. As in the previous case for $M = 0$ in Sec. IV, now for $M = 1$ in Fig. 7(a) step $n = 1$ also exhibits branching. If we analyze the voltage-time dependence, for

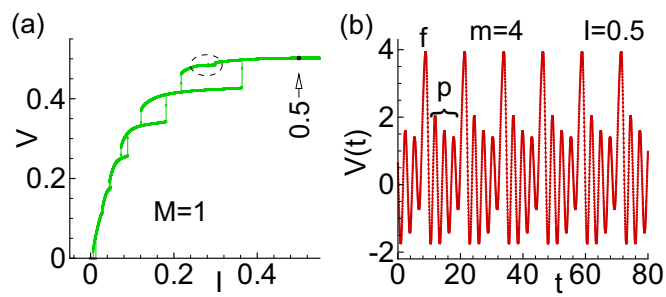

FIG. 7. (a) I-V curve of the AAJJ for $M = 1$ in the region of the step $n = 1$ for the one-fluxon state. (b) Voltage-time dependence at the upper branch of the one-fluxon zero-field step for the current value marked by the arrow.

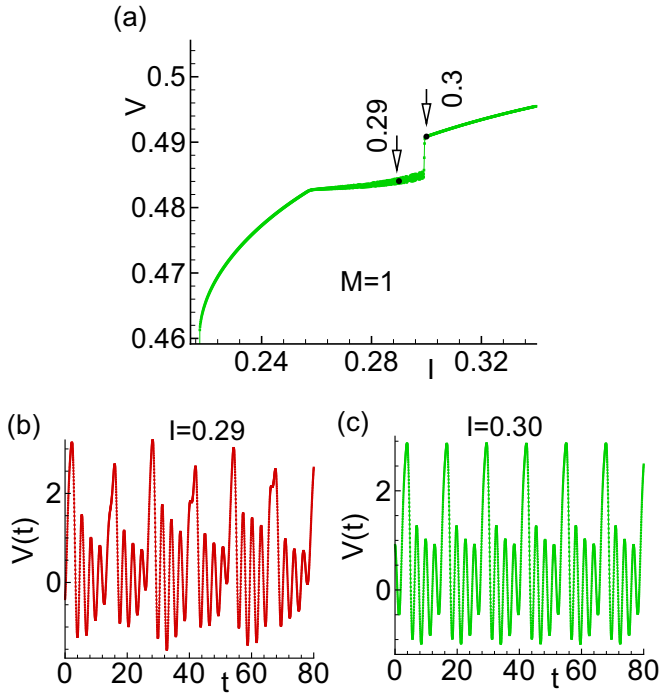

FIG. 8. (a) High-resolution plot of the area within the dashed circle in Fig. 7(a). Voltage-time dependence at (b) $I = 0.29$ and (c) $I = 0.3$.

example, for a given value of I marked by the arrow at step $n = 1$ in Fig. 7(a), we can see in Fig. 7 (b) that the upper branch corresponds to the fluxon passing at every fourth plasma oscillation.

However, besides branching, when $M = 1$ the step in Fig. 7(a) exhibits an interesting feature (an additional branch), enclosed by the dashed circle, which does not appear in the I-V characteristics of the AAJJ with no trapped fluxons ($M = 0$). In Fig. 8, a high-resolution plot of the area within the dashed circle in Fig. 7(a) and the corresponding voltage-time dependence at two values of current I for the AAJJ with one trapped fluxon ($n = 1$) are presented. Looking at Fig. 8(a), at first it might seem that there is an additional branch, nevertheless, the voltage-time dependence at the two current values marked by arrows in Figs. 8(b) and 8(c) shows that in both cases we have resonance of order $m = 4$ (the fluxon passes every fourth plasma oscillation). However, in Fig. 8(b) for the current value $I = 0.29$, we can clearly see changes in the maxima corresponding to the fluxon, which we therefore call a *pulsating fluxon*. The observed feature is a result of the resonance between the pulsating fluxon and the Josephson frequency. We performed simulations for different system parameters and discovered that this phenomenon existed only in the underdamped case and disappeared as damping was increased.

VII. COMPARATIVE ANALYSIS OF THE I-V CHARACTERISTICS FOR $M = 0$ AND $M = 2$

In order to further examine how the type of excitations affects the AAJJ, let us compare two cases: $M = 0$ and $M = 2$. At first one might expect that the I-V characteristics for $M = 0$ and $M = 2$ should be the same since in both cases

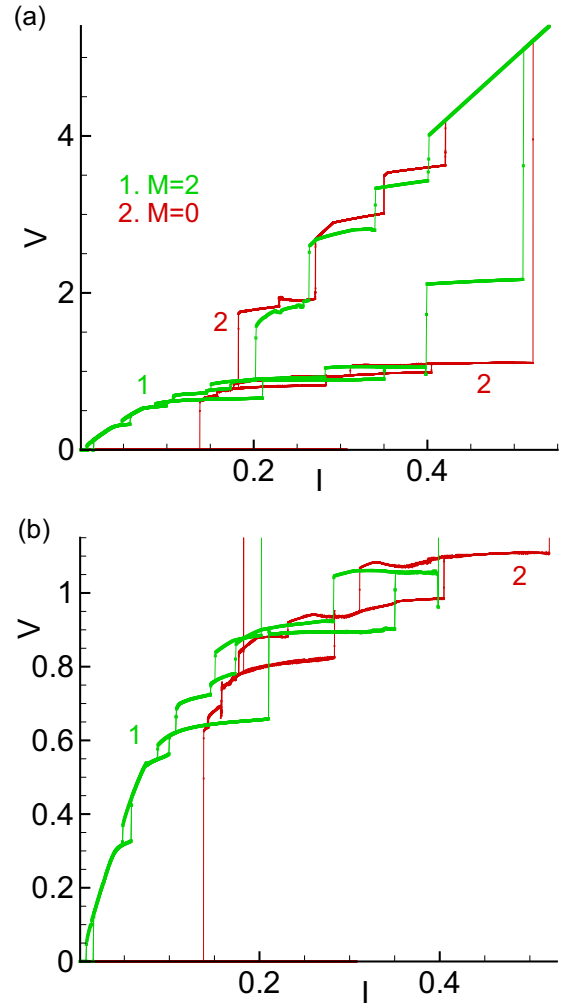

FIG. 9. (a) I-V characteristics of the AAJJ for $N = 10$, $a = 1$, $\alpha = 0.1$, and $M = 0$ (red) and $M = 2$ (green). (b) High-resolution plot of the $n = 2$ step.

ZFSs appear at $n = 2, 4, 6$, and 8, however, this is not the case. In Fig. 9, the I-V characteristics for the case $M = 0$, with no trapped fluxon, and the case $M = 2$, with two trapped fluxons, are presented. As we can see in Fig. 9(a), the steps are shifted with respect to each other. At the ZFS $n = 2$, for $M = 0$ we have one fluxon and one antifluxon, while for $M = 2$ we have two fluxons. At the next step, $n = 4$, we will have two fluxons and two antifluxons for $M = 0$, while for $M = 2$ there will be three fluxons and one antifluxon, etc. So, although the total number of excitations n is the same for both values of M, the numbers of fluxons and antifluxons are different. For $M = 0$ we always have the same number of fluxons and antifluxons, $n_f = n_{\rm af}$, while for $M = 2$, in addition to fluxon-antifluxon pairs we have two trapped fluxons, so that $n_f \neq n_{\rm af}$, and this completely changes the dynamics of the system.

In the high-resolution plot of step $n = 2$ presented in Fig. 9(b), we can also see that for $M = 2$ the voltage goes to 0 as I goes to 0, while for $M = 0$ the voltage goes to 0 around $I = 0.14$. This stems from that fact that for $M = 0$, a fluxon-antifluxon pair can exist only above some critical current. So, when I becomes smaller than that value, there are

no fluxon-antifluxon pairs, and consequently, V drops to 0. On the other hand, if we have two trapped fluxons, they will be moving as long as $I \neq 0$, and as I goes to 0, their speed and, consequently, the voltage will go to 0.

VIII. CONCLUSION

In this work, the resonance phenomena in the absence of external radiation in an annular array of Josephson junctions have been analyzed in a wide range of currents and voltages for different numbers and types of excitations present in the system: from the case of no trapped fluxons, i.e., circulating fluxon-antifluxon pairs, to the cases of trapped fluxons and their simultaneous motion with the pairs. The obtained results showed that the appearance and the number of zero-field steps were determined by the number of junctions and the excitations present in the system. A high-resolution analysis of the current-voltage characteristics showed that the branching of zero-field steps due to locking between rotating excitations and plasma oscillations in their tails was the most prominent at the lowest step and, as the number of excitations increased, gradually disappeared at the higher steps. A comparative analysis between two different systems, one without and one with one trapped fluxon, revealed a correlation between the two current-voltage characteristics. In the case of one trapped fluxon, in the region of the first (lowest) zero-field step, a special feature, i.e., an additional branch, was observed, which appeared as a signature of the pulsating fluxon resonating at the Josephson frequency. Examination of systems with the same total number but different types of excitations showed that the dynamics of the AAJJ was determined not only by the number, but also by the type of excitations, i.e., the current-voltage characteristics differed depending on the type of excitations. In other words, a system with one fluxon and one antifluxon, for example, does not behave the same as a system with two trapped fluxons, although the total number of excitations is the same.

All these phenomena that we observed are not just related to this particular system of Josephson junctions, annular geometry, or zero-field steps but could be relevant for a wide variety of underdamped Josephson junction systems, which can exhibit resonance, interference, and other frequency locking phenomena based on the flux-quanta motion [43–45]. Regarding the relevance of our results for other frequency locking phenomena, such as, for example, Shapiro steps, we just showed, in a separate study of an underdamped Josephson junction system under external radiation, that the ability of the system to exhibit Shapiro steps was determined not just by the number but also by the type of excitations circulating in the system [46].

Annular Josephson junctions possess an enormous potential for various technological applications [1]. Superconducting digital technology is capable of achieving much higher energy efficiencies than other technologies [10–18], and fluxon dynamics as well as resonance phenomena are at the core of some of the most advanced ideas in these fields. Another interesting application of annular Josephson junctions is in superconducting metamaterials with a number of unique properties, which are difficult to achieve in any other way [19]. A generic element of such a material is a superconducting ring split by a Josephson junction, and one of the most recent theoretical and experimental studies is dedicated to the resonant response of such metamaterials to the external signal in strongly nonlinear regimes [19]. Regardless of the field in which annular Josephson junctions have application, a good understanding of their dynamics is crucial. For this reason, the resonance phenomena that we have presented require further experimental examination, which we will report in the future.

ACKNOWLEDGMENTS

J.T. wishes to thank the Bogoliubov Laboratory of Theoretical Physics, Joint Institute for Nuclear Research, Dubna, Russia, where some of this work was done, for their generous hospitality. This work was supported by the Foundation for the Advancement of Theoretical Physics and Mathematics "Basis." The reported study was funded by Russian Foundation for Basic Research (RFBR) research Projects No. 18-02-00318 and No. 18-52-45011-IND. Numerical simulation was funded by Russian Science Foundation (RSF) Project No. 18-71-10095. The research was funded by the Ministry of Education, Science and Technological Development of the Republic of Serbia. This work was supported by the Ministry of Education, Science and Technological Development of the Republic of Serbia under the Contract No. 451-03-68/2020-14/200125 and by the Provincial Secretariat for High Education and Scientific Research of Vojvodina (Project No. APV 114-451-2201).

[1] J. J. Mazo and A. V. Ustinov, *The Sine-Gordon Model and Its Applications* (Springer, Cham, Switzerland, 2014).
[2] O. Braun and Yu. S. Kivshar, *The Frenkel-Kontorova Model* (Springer, Berlin, 2003).
[3] J. Tekić and P. Mali, *The AC Driven Frenkel-Kontorova Model* (University of Novi Sad, Novi Sad, 2015).
[4] L. M. Floría and J. J. Mazo, Adv. Phys. **45**, 505 (1996).
[5] T. A. Fulton and R. C. Dynes, Solid State Commun. **12**, 57 (1973).
[6] D. W. McLaughlin and A. C. Scott, Phys. Rev. A **18**, 1652 (1978).
[7] M. Lucci, D. Badoni, V. Merlo, I. Ottaviani, G. Salina, M. Cirillo, A. V. Ustinov, and D. Winkler, Phys. Rev. Lett. **115**, 107002 (2015).
[8] J. Clarke, Nature **425**, 133 (2003).
[9] A. Wallraff, A. Lukashenko, J. Lisenfeld, A. Kemp, M. V. Fistul, Y. Koval, and A. V. Ustinov, Nature **425**, 155 (2003).
[10] K. G. Fedorov, A. V. Shcherbakova, M. J. Wolf, D. Beckmann, and A. V. Ustinov, Phys. Rev. Lett. **112**, 160502 (2014).
[11] K. K. Likharev and V. K. Semenov, IEEE Trans. Appl. Supercond. **1**, 3 (1991).
[12] O. A. Mukhanov, IEEE Trans. Appl. Supercond. **21**, 760 (2011).
[13] J. Ren and V. K. Semenov, IEEE Trans. Appl. Supercond. **21**, 780 (2011).
[14] V. K. Semenov, G. V. Danilov, and D. V. Averin, IEEE Trans. Appl. Supercond. **13**, 938 (2003).

[15] M. H. Volkmann, A. Sahu, C. J. Fourie, and O. A. Mukhanov, Supercond. Sci. Technol. **26**, 015002 (2013).
[16] M. Cirillo, J. Appl. Phys. **58**, 3217 (1985).
[17] N. Takeuchi, Y. Yamanashi, and N. Yoshikawa, Supercond. Sci. Technol. **28**, 015003 (2015).
[18] Q. P. Herr, A. Y. Herr, O. T. Oberg, and A. G. Ioannidis, J. Appl. Phys. **109**, 103903 (2011).
[19] E. I. Kiselev, A. S. Averkin, M. V. Fistul, V. P. Koshelets, and A. V. Ustinov, Phys. Rev. Research **1**, 033096 (2019).
[20] P. Crotty, D. Schult, and K. Segall, Phys. Rev. E **82**, 011914 (2010).
[21] M. Remoissenet, *Waves Called Solitons: Concepts and Experiments*, (Springer, Berlin, 1999).
[22] S. N. Emé and R. D. Pamentier, J. Appl. Phys. **51**, 5025 (1980).
[23] M. Cirillo, B. H. Larsen, A. V. Ustinov, V. Merlo, V. A. Oboznov, and R. Leoni, Phys. Lett. A **183**, 383 (1993).
[24] A. Davidson, B. Dueholm, B. Kryger, and N. F. Pedersen, Phys. Rev. Lett. **55**, 2059 (1985).
[25] J. Pfeiffer, A. A. Abdumalikov, Jr., M. Schuster, and A. V. Ustinov, Phys. Rev. B **77**, 024511 (2008).
[26] J. Pfeiffer, M. Schuster, A. A. Abdumalikov, and A. V. Ustinov, Phys. Rev. Lett. **96**, 034103 (2006).
[27] A. V. Ustinov, M. Cirillo, and B. A. Malomed, Phys. Rev. B **47**, 8357 (1993).
[28] A. V. Ustinov, T. Doderer, R. P. Huebener, N. F. Pedersen, B. Mayer, and V. A. Oboznov, Phys. Rev. Lett. **69**, 1815 (1992).
[29] H. S. J. van der Zant, T. P. Orlando, S. Watanabe, and S. H. Strogatz, Phys. Rev. Lett. **74**, 174 (1995).
[30] A. Wallraff, A. V. Ustinov, V. V. Kurin, I. A. Shereshevsky, and N. K. Vdovicheva, Phys. Rev. Lett. **84**, 151 (2000).
[31] I. V. Vernik, V. A. Obozonov, and A. V. Ustinov, Phys. Lett. A **168**, 319 (1992).
[32] S. Watanabe, S. H. Strogatz, H. S. J. van der Zant, and T. P. Orlando, Phys. Rev. Lett. **74**, 379 (1995).
[33] C. Nappi, M. P. Lisitskiy, G. Rotoli, R. Cristiano, and A. Barone, Phys. Rev. Lett. **93**, 187001 (2004).
[34] R. Monaco, J. Mygind, and V. P. Koshelets, Phys. Rev. B **100**, 064501 (2019).
[35] P. S. Lomdhal, O. H. Soerensen, and P. L. Christiansen, Phys. Scripta **25**, 879 (1982).
[36] H. Kawamoto, Prog. Theor. Phys. **70**, 1171 (1983).
[37] A. C. Scott and W. J. Johnson, Appl. Phys. Lett. **14**, 316 (1969).
[38] D. E. McCumber, J. Appl. Phys. **39**, 3113 (1968).
[39] W. C. Stewart, Appl. Phys. Lett. **12**, 277 (1968).
[40] A. V. Ustinov, Physica D **123**, 315 (1998).
[41] Yu. Shukrinov, I. Rahmonov, and M. Hamdipour, Lect. Notes Comput. Sci. **7125**, 234 (2012).
[42] Yu. M. Shukrinov, I. R. Rahmonov, JETP **115**, 289 (2012).
[43] P. Solinas, S. Gasparinetti, D. Golubev, and F. Giazotto, Sci. Rep. **5**, 12260 (2015).
[44] M. Lucci, D. Badoni, V. Corato1, V. Merlo, I. Ottaviani, G. Salina, M. Cirillo, A. V. Ustinov, and D. Winkler, J. Phys. D: Appl. Phys. **49**, 065303 (2016).
[45] O. V. Pountougnigni, R. Yamapi, G. Filatrella, and C. Tchawoua, Phys. Rev. E **99**, 032220 (2019).
[46] I. R. Rahmonov, J. Tekić, P. Mali, A. Irie, and Yu. M. Shukrinov, Phys. Rev. B **101**, 024512 (2020).